

# AUTONOMOUS AERIAL OBSERVATION SYSTEM FOR DISASTER RESPONSE USING ELECTRIC DUCTED FAN MAVS

**Naoki Nagasaka , Daisuke Kubo**

**Department of Aeronautics and Astronautics, University of Tokyo  
7-3-1, Hongo, Bunkyo-ku, Tokyo 113-8656, Japan**

**Keywords:** *VTOL, MAV, Ducted fan, Aerial photography, Disaster management*

## Abstract

We propose a new distributed disaster observation system using electric ducted fan (EDF) propelled vertical take-off and landing (VTOL) micro aerial vehicles (MAVs). We term the system “Low Cost Aerial Photography System (LCAPS).” The EDF VTOL MAV’s dynamics were modeled and simulated. A prototype was developed and its basic performance was verified through tethered flight testing.

## 1 Introduction

Japan is one of the most earthquake-prone countries in the world, because there are four tectonic plates meeting around the Japanese archipelago. In 2002, the Munich Reinsurance Company reported that the Tokyo–Yokohama conurbation in Japan was the megacity having the highest level of risk for natural catastrophes including earthquakes[1, 2]. This risk estimation was based on hazard occurrence probability, vulnerability to the hazards, and the influence on the economy. To reduce the damage of future big earthquakes, countermeasures must be developed as soon as possible.

In Japan, when there is a big earthquake, the disaster response headquarters is to be set up within approximately one hour after the occurrence of the earthquake. At this time, the availability of extensive and detailed information about the damage can make a crucial difference for disaster response planning

at the headquarters. However, there are currently no practical methods to quantify the damage of the earthquake in such an early phase, because conventional aerial observation methods—manned airplanes, helicopters, and observation satellites—require a long time to reach the disaster area. The damage of an earthquake can be roughly estimated just after its occurrence by a rapid simulation system called “Early Estimation System (EES),” which is developed and operated by the Cabinet Office of the Japanese government[3]. However, from past experience in application to real earthquakes, it appeared that this system is not so accurate; there were large differences between the predicted and the actual number of casualties. Therefore, it is still very important to obtain hard information such as aerial photographs. The combination of these two systems—prediction and observation—can provide very valuable information for disaster mitigation.

We propose a system for rapid and accurate information acquisition, termed “Low Cost Aerial Photography System (LCAPS)[4].” This system consists of a number of simple and low cost micro aerial vehicles (MAVs) and ground stations (GSs). The MAV is equipped with a digital camera and wireless communication system. The MAVs take aerial photographs just after the occurrence of an earthquake and transmit the photographs to the GSs. At the GSs, photographic data are processed and large but detailed hazard maps can be constructed. This system is cheaper and faster than any other

conventional observation method.

We propose an electric ducted fan (EDF) propelled vertical take-off and landing (VTOL) MAV as the observation platform for the LCAPS concept. It has several advantages such as small installation space, all-weather operation, and easy maintenance. Fuel-powered vehicles are not suitable for the LCAPS concept because they are too heavy. The proposed electric-powered vehicle has short endurance compared to fuel-powered ones. However, that is not a big problem because the LCAPS concept requires only short endurance.

In the remainder of this paper, we first propose the LCAPS concept (section 2). Next, we compare aerial platforms for the concept, propose the EDF propelled MAV, and introduce a prototype (section 3). The vehicle's simulation model is constructed in section 4 and its flight characteristics are simulated. In section 5, we discuss flight tests using the prototype. Finally, we conclude this paper in section 6.

## 2 Low Cost Aerial Photography System

### 2.1 Overview of LCAPS

We will now provide an overview of LCAPS. A number of MAVs and their launch bases are permanently deployed over densely populated and high-risk areas. The launch bases keep the vehicle's batteries charged until flight, offer a protective cover which opens during operation, and receive earthquake intensity information. When an earthquake stronger than a pre-set threshold occurs, the MAVs launch from their bases, climb to a certain altitude, and take photographs fully autonomously. Several GSs, also deployed over the area, gather the aerial photographs from the vehicles via wireless communication and process the images to obtain feature quantities such as the rate of collapsed buildings and the damage level. Finally the GSs transmit the data to the disaster headquarters and other agencies via a disaster communications network (i.e., a ground or satellite communication network).

These processes happen quickly and disaster headquarters can get the information rapidly, so that rescue work can be organized more and more efficiently. Additionally, the obtained information can be used by evacuees to avoid dangerous sites if it is directly broadcasted, for example, to their mobile phones.

### 2.2 Features and advantages of LCAPS

Important points in this study are “fully autonomous,” “distributed observation,” using “low cost,” and “simple” aerial platforms. We use multiple MAVs simultaneously to take aerial photographs of disaster areas, and the whole system works fully autonomously. This concept has the following advantages compared to a system using a small number of higher-performance and expensive platforms.

#### a) High system robustness

Distributed systems have high robustness because of redundancy. Even if some of the vehicles cannot operate correctly, other vehicles placed near the defective vehicles can serve as a replacement.

#### b) Rapid availability of aerial photographs

The system gathers photographs of the disaster area rapidly because many vehicles covering the whole area can take photographs concurrently. A small number of sophisticated vehicles will need more time to cover the same area.

#### c) Flight safety because of their small size

The safety of the system is very important because we generally want to obtain information especially in densely populated areas. Considering this, a system using small and light platforms is better than a system using large and heavy platforms. Heavy vehicles are not preferred, because it is dangerous to the ground in case of failure. Secondary damages or injuries are not acceptable.

#### d) Manufacturing: economy of scale

Generally, we can save manufacturing cost because of the economy of scale. The LCAPS consists of a large number of uniform MAVs. Therefore, it is possible to reduce the total cost of the system.

**2.3 Detailed operating flow of LCAPS**

The operating flow of LCAPS is illustrated in Fig. 1. It is mainly divided into two flows, i.e., one for the MAVs and one for the GSs.

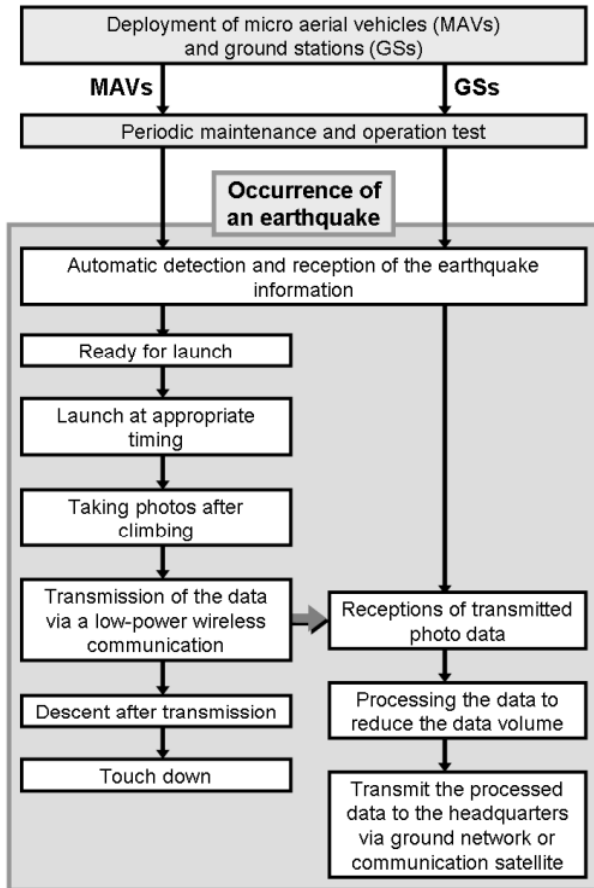


**Fig. 1** Operation flow chart of LCAPS

**a) Aerial platforms**

The MAVs are located at a certain distance from each other, considering performance of data transfer, photo quality, and flight altitude. The installation sites of the vehicles can be the roofs of public buildings such as hospitals or schools, because these buildings are usually well built and the system will be less likely to get damaged.

The system receives information of earthquake intensity, and comes into operation automatically. After that, the MAVs get ready for their launches—open the protective cover, fully charge their batteries, and initialize their autopilot systems. They launch at the

most effective timing to get the most useful information. For example, just after the occurrence of an earthquake, there may be collapsed buildings, but fires may not have broken out yet.

The vehicles climb to a certain altitude. The altitude will have to be decided regarding the legal restrictions and civil aviation law of each country. After reaching the altitude, each vehicle stabilizes its attitude and takes an aerial photograph using an on-board digital camera.

The vehicle keeps flying until the photograph data have been transmitted to a GS, because it is better to maintain a line of sight to the GS during transmitting data using a low power wireless communication. As the distance between the vehicle and the GS is short, small, low emission power radio modems are sufficient. After transmitting the data, the vehicle descends vertically and touches down.

**b) Ground stations**

GSs are also deployed all over the concerned area from ordinary times. One GS receives photographic data from multiple vehicles, and the data is transmitted to the disaster headquarters using some available communication line. Several types of communication lines are candidates for this application. For example, ground wired communication lines, ground based wireless communication lines, and satellite communication lines. However, satellite communications are preferable for the LCAPS concept, because ground communications can be damaged by an earthquake.

Considering the bandwidth of the communication lines, it is better to process the data at each GS to reduce the data volume. Even if initially only the feature quantities of the photographs (e.g., damage level, collapsed rate, and number of detected fires) are available to the headquarters, it is also beneficial for initial disaster response planning. The original data can be transmitted after the completion of the transmission of the feature quantities. This strategy is also beneficial from a viewpoint of distributed processing to reduce processing load concentrated to central system (i.e., the disaster

headquarters).

### 3 Small Aerial Observation Platform

#### 3.1 Requirements for the platform

There are many candidates for an unmanned aerial observation platform, such as airplanes, helicopters, and blimps. These candidates have both advantages and disadvantages as an aerial observation platform for various types of missions; which platform is most suitable strongly depends on the mission characteristics. For this emergency observation system, i.e., the LCAPS concept, the following requirements exist for the platform:

- Small installation space
- All-weather operation
- Easy maintenance.

Considering these points, we propose a single EDF propelled VTOL MAV (Fig. 2) as the LCAPS platform. The proposed vehicle has a configuration typical for a single ducted fan propulsive vehicle; it has a single ducted fan at the center of the body, control vanes on the lower side of the duct, and landing gears around the vanes.

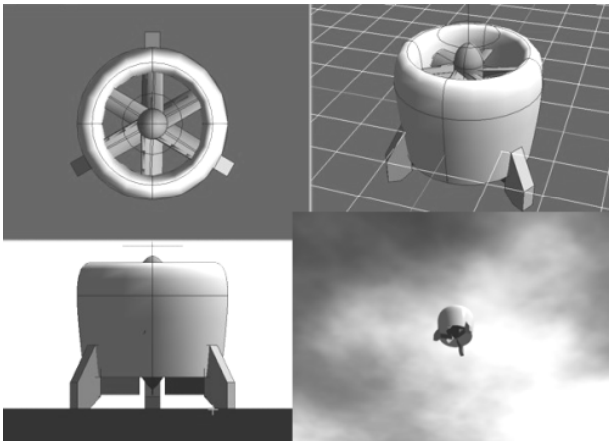


**Fig. 2** Concept image of the EDF VTOL MAV

VTOL capability is favorable to minimize installation and launch space, and EDF MAVs

are robust to wind gusts because of their high disk loading. Of course, helicopters with high disk loading may be possible, but they would be complicated to make and difficult to maintain. The ducted fan mechanism on the other hand is very simple and easy to maintain.

Although a helicopter might be superior to an EDF VTOL MAV with respect to maneuverability, maneuverability is not required in this operation concept. As for the endurance, an EDF is inferior to other platforms, because its flight efficiency is relatively low. However, the LCAPS concept does not require high endurance because it focuses on disaster information gathering especially in the early phase of an earthquake disaster.

The safety of the platform is also an important requirement. It should be designed as ground-safe. Since MAVs are relatively small and have only low kinetic energy in their flight, they are generally suitable for such a disaster observation mission. However, an EDF MAV does not have any mechanism in case of power failure, whereas other platforms do. For example, airplanes can glide without propulsion, airships can keep floating without power, and helicopters have a no-power safety landing ability called autorotation. A plain EDF MAV is therefore inferior to other platforms with respect to safety. However, the problem can easily be solved by equipping it with a parachute and designing the outer surface of the vehicle using soft materials.

#### 3.2 Prototype EDF MAV

A prototype (Fig. 3) was constructed using a ducted fan system that was designed and manufactured in this research.

The prototype's fan diameter is 15 cm and the height is 40 cm. The duct is made of carbon fiber reinforced plastic. A small autopilot system, which consists of a GPS receiver, 3-axis accelerometers, 3-axis gyros, and a 150 MIPS microprocessor is installed above the duct. Four control vanes are equipped under the duct. The flying weight is 600 g and the maximum thrust is 900g. The weight breakdown is listed in Table 1.

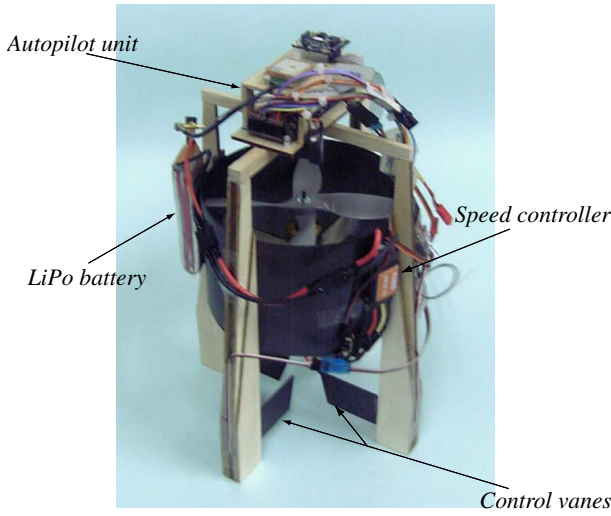


**Fig. 3** Prototype of the EDF MAV

**Table 1** Component weights of the prototype

| Component               | Weight[g] |
|-------------------------|-----------|
| CFRP duct               | 74        |
| Landing gears           | 60        |
| Electric motor          | 58        |
| Motor controller        | 30        |
| Propeller               | 16        |
| Lithium-polimer battery | 130       |
| Vanes and servo motors  | 46        |
| Autopilot               | 116       |
| Receiver                | 16        |
| Others (cabling etc.)   | 54        |
| Total                   | 600       |

## 4 Modeling and Flight Simulation

### 4.1 Modeling of EDF MAV dynamics

A mathematical model was constructed to study the vehicle's flight characteristics and to design the flight controller for flight testing of the prototype vehicle. In this study, accuracy of the mathematical modeling is not essential because the objective is to demonstrate the concept of

the EDF MAV. Even simple models are sufficient to analyze the qualitative characteristics of the vehicle.

In this study, the following six degrees of freedom dynamical equations are used:

$$\begin{aligned} m\dot{\mathbf{V}} &= \mathbf{F} \\ \dot{\mathbf{h}} &= \mathbf{M} \end{aligned}$$

where  $\mathbf{F}$  and  $\mathbf{M}$  represent respectively the vector of forces and torques applied to the vehicle expressed in the body frame,  $m$  represents the total vehicle mass, and  $\mathbf{h}$  represents the angular momentum vector. The external force vector  $\mathbf{F}$  is divided into the following four terms:

$$\mathbf{F} = \mathbf{F}_{fan} + \mathbf{F}_{drag} + \mathbf{F}_{vane} + \mathbf{F}_{grav}$$

where  $\mathbf{F}_{fan}$  is the thrust force produced by the ducted fan,  $\mathbf{F}_{drag}$  is the drag force acting on the body of a vehicle,  $\mathbf{F}_{vane}$  is the aerodynamic force acting on the control vanes, and  $\mathbf{F}_{grav}$  is the gravitational force. Although there are interfering forces among these terms in actual aerodynamic phenomena, they are eliminated in this study; it is a future work to analyze the detail of these aerodynamic phenomena. The external moment vector  $\mathbf{M}$  is also divided into four terms:

$$\mathbf{M} = \mathbf{M}_{fan} + \mathbf{M}_{drag} + \mathbf{M}_{vane} + \mathbf{M}_{gyro}$$

where  $\mathbf{M}_{fan}$ ,  $\mathbf{M}_{drag}$ , and  $\mathbf{M}_{vane}$  are defined similar to the external force terms  $\mathbf{F}_{fan}$ ,  $\mathbf{F}_{drag}$ , and  $\mathbf{F}_{vane}$ , and  $\mathbf{M}_{gyro}$  is the gyro effect term caused by the propeller rotation. Although there are interfering terms in actual phenomena, they are also eliminated here similar to the interference of external forces. In the calculation of the aerodynamic forces and moments acting on the body of the vehicle, projected areas to each coordinate plane are used as reference areas. The drag forces are assumed to act on the center of gravity of the vehicle.  $\mathbf{F}_{fan}$  and  $\mathbf{M}_{fan}$  are calculated using the blade element momentum theorem. Using this method, the ducted fan thrust, momentum, and induced velocity are connected to the propeller rotation speed  $\Omega$ . The thrust component generated by the pressure

distribution on the duct lip is ignored in this paper. In this paper, the throttle setting is kept at full position in all flight simulations. Therefore, the rotation speed can be considered near constant, and the gyro effect can be written as[5]:

$$\mathbf{M}_{gyro} = -\boldsymbol{\omega} \times \mathbf{h}_{rot}$$

where  $\boldsymbol{\omega}$  is the angular velocity of the vehicle and  $\mathbf{h}_{rot}$  is the angular momentum vector of the rotating part of the vehicle, i.e., motor rotator, propeller, and spinner. All the parameters of the mathematical model are set using actual values of the prototype vehicle (Fig. 3).

## 4.2 Control System Architecture

In order to simplify the control system, only three virtual control inputs  $\mathbf{u} = [u_1, u_2, u_3]^T$  are considered in the controller design. These virtual inputs are used to control yaw angle, pitch angle, and roll angle, respectively.

The actual control inputs—deflection angles of vanes  $\boldsymbol{\delta} = [\delta_1, \delta_2, \delta_3, \delta_4]^T$ —are obtained by mixing the virtual inputs  $\mathbf{u}$ . This mixing law is given as:

$$\begin{aligned} \delta_1 &= -u_2 - u_3 \\ \delta_2 &= -u_1 - u_3 \\ \delta_3 &= u_2 - u_3 \\ \delta_4 &= u_1 - u_3. \end{aligned}$$

The coordinates and the positive direction of vane deflections are defined in Fig. 4.

The control system architecture is illustrated in Fig. 5. The inner-loop controller is used to stabilize and track attitude command signals generated by the outer-loop controller, and the outer-loop controller is designed to maintain a commanded horizontal speed. The yaw angle command  $\psi_c$  is assumed to be given as a constant. The throttle setting  $\delta_{thr}$  is set to the maximum value on a constant basis in the flight. Feedback gain values are determined by a trial and error method.

In the control architecture illustrated in Fig. 5, the inner-loop attitude controller is given by

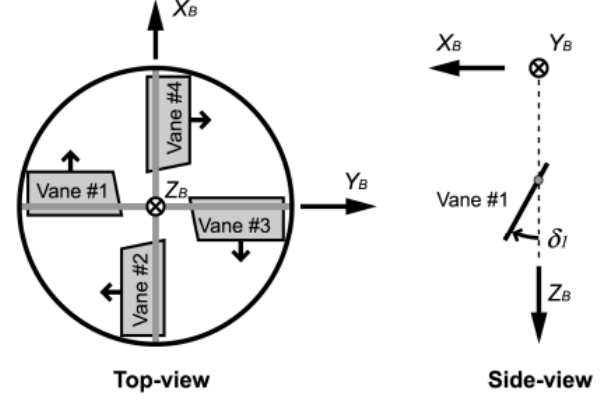


Fig. 4 Definition of deflection angle of vanes

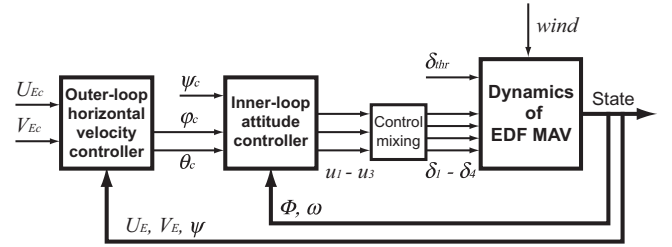


Fig. 5 Block diagram of the control system

the following equation:

$$\mathbf{u} = \mathbf{K}_P(\boldsymbol{\Phi} - \boldsymbol{\Phi}_c) + \mathbf{K}_I \int (\boldsymbol{\Phi} - \boldsymbol{\Phi}_c) dt + \mathbf{K}_D \boldsymbol{\omega}$$

where  $\mathbf{K}_P$ ,  $\mathbf{K}_I$  and  $\mathbf{K}_D$  are gain matrixes,  $\boldsymbol{\Phi}$  is the euler angle defined as  $\boldsymbol{\Phi} = [\phi, \theta, \psi]^T$ , and  $\boldsymbol{\Phi}_c$  is the euler angle command .

The equation for the outer-loop horizontal velocity controller is as follows:

$$\begin{bmatrix} \theta_c & \phi_c \end{bmatrix}^T = \mathbf{K}_{VP}(\mathbf{V}_H - \mathbf{V}_{Hc}) + \mathbf{K}_{VI} \int (\mathbf{V}_H - \mathbf{V}_{Hc}) dt$$

where  $\mathbf{K}_{VP}$  and  $\mathbf{K}_{VI}$  are gain matrixes,  $\theta_c$  and  $\phi_c$  are attitude commands, and  $\mathbf{V}_H$  and  $\mathbf{V}_{Hc}$  are horizontal ground velocity and commands, respectively, which are defined as follows:

$$\mathbf{V}_H = \begin{bmatrix} U_H \\ V_H \end{bmatrix} = \begin{bmatrix} U_E \cos \psi + V_E \sin \psi \\ -V_E \sin \psi + U_E \cos \psi \end{bmatrix}$$

where  $U_E$  and  $V_E$  are ground velocity components defined in the inertial frame.

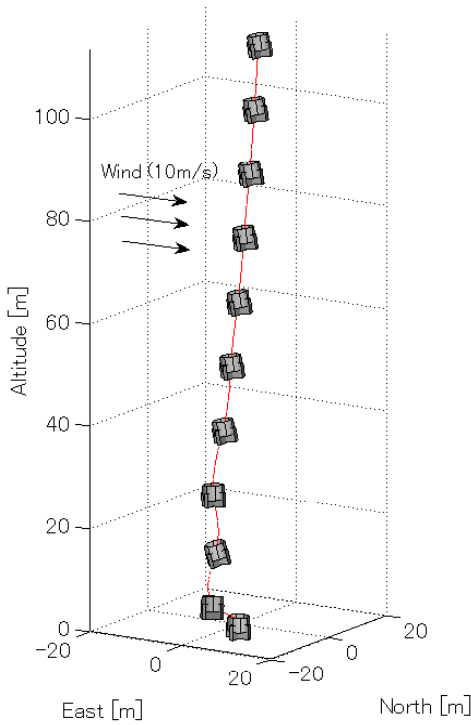
When the proposed flight controller (Fig. 5) is applied to the actual EDF MAV, GPS velocity is to be used as  $U_E$  and  $V_E$ . Therefore, in the simulations described below, GPS sampling rate (4Hz) and delay (0.25s) are also modeled.

### 4.3 Simulation Result

We simulated a 20-second climbing flight using the mathematical model described above. Simulation conditions are given in Table 2, and results are shown in Figs. 6, 7, and 8.

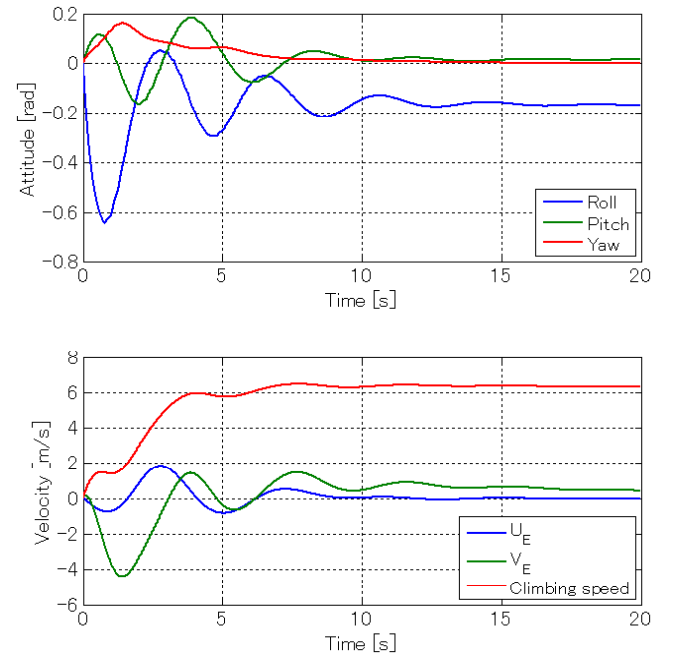
**Table 2** Simulation condition

|                |                     |   |
|----------------|---------------------|---|
| Initial values | Velocity            | $\mathbf{V} = [0, 0, 0]^T$ m/s            |
|                | Angular velocity    | $\boldsymbol{\omega} = [0, 0, 0]^T$ rad/s |
|                | Euler angle         | $\boldsymbol{\Phi} = [0, 0, 0]^T$ rad     |
| Commands       | Horizontal velocity | $U_{Ec} = 0$ m/s<br>$V_{Ec} = 0$ m/s      |
|                | Yaw angle           | $\psi_c = 0$ rad                          |
| Wind           |                     | $\mathbf{V}_{wind} = [0, 10, 0]^T$ m/s    |



**Fig. 6** Flight simulation result

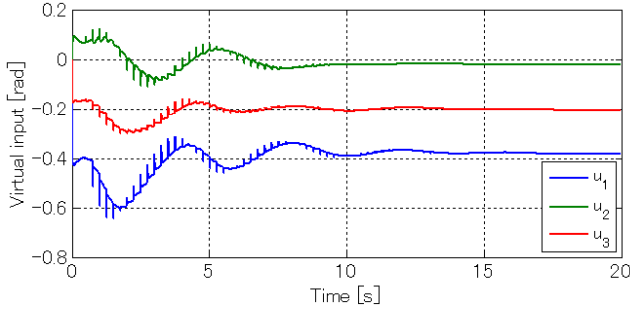
In Fig. 6, the continuous red line is the flight path of the EDF MAV, and the vehicle illustrations show the attitude at intervals of two seconds. First, the vehicle tilts windward because of weathercock stability and then climbs diagonally. However, the attitude of the vehicle is rapidly regulated and the horizontal velocity is controlled to nearly zero. Although the PID controller designed in this study is very simple, it is useful to control the EDF MAV.



**Fig. 7** State variables

Fig. 7 shows the state variables of the vehicle. The pitch angle  $\theta$  and the yaw angle  $\psi$  are controlled to 0 rad. On the other hand, the roll angle  $\phi$  converges to 0.16 rad in order to fly against the 10 m/s static wind from the West. Under the simulation condition, the terminal climbing speed is about 6 m/s.

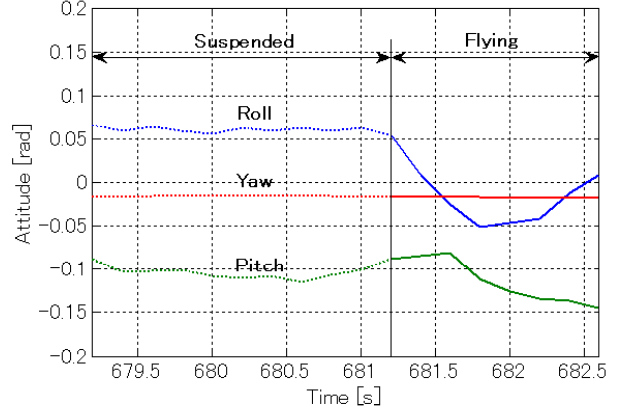
Fig. 8 shows the virtual control inputs. During the short time after the launch, all three lines lack smoothness. This is because the GPS velocity for the outer-loop controller is updated at a rate of 4Hz. However, a short time later, horizontal ground velocity is controlled to nearly zero and the spikes on the virtual inputs disappear. Among the virtual inputs,  $u_3$ ,


**Fig. 8** Virtual inputs

which controls yaw angle, can be minimized, because the stators fixed inside of the duct can generate torque to counteract the antitorque of the propeller if they are properly designed. In this study, the torque from these stators are not modeled for the sake of simplicity.

## 5 Flight Testing

A tethered flight test of the prototype vehicle was carried out in our laboratory. During this flight, the vehicle was attached to a tether, which connected to the ceiling for safety. The line was kept slack in flight. Only the attitude was controlled using a MicroPilot MP2128 [6]; the horizontal velocity was not controlled. A human pilot operated the throttle of the EDF remotely. The vehicle successfully flew, which is shown in Fig. 10. First, the throttle was tuned to keep the flight altitude, and after a few second, the throttle was raised; the vehicle accelerated and climbed to a height of 3 m. The time-history of the vehicle's attitude is illustrated in Fig. 9; the lateral axis is the elapsed time from the beginning of data recording. The solid line is the flying period and the dashed line is the suspended period. The vehicle is flying from elapsed time 681.2 s to 682.6 s. The vehicle attitude was not divergent in this short-time flight test, but we are planning a flight test with extended flight time for further validation.


**Fig. 9** Attitude during flight

## 6 Conclusions and Future Work

A new distributed aerial observation concept for disaster mitigation termed LCAPS was proposed. This system is cheaper and faster than any other conventional method. An EDF MAV was proposed as the platform vehicle for LCAPS, and the dynamics was modeled and simulated. On the basis of this simulation, we carried out flight tests with the prototype vehicle; tethered flights have been successfully conducted using only an attitude controller and manually operated throttle. Through these flight tests, a proof of concept was given and the effectiveness of the attitude controller have been validated .

For the next step, we will validate the horizontal velocity controller through hovering flight testings. However, we currently still have problems regarding the sensitivity and accuracy of the GPS module. After testing several GPS antennas, we concluded that there seems to be an electrical interference between the micro processing unit (MPU) and GPS antennas. In order to improve GPS sensitivity, we are now planning to shield MPU or relocate components. After solving these problems, we will equip the prototype with a digital camera and a parachute, and conduct free flight test. Finally, the full mission flight—autonomous flight, aerial photography, data transfer, and processing—will be demonstrated in the future.

**References**

- [1] *Topics geo annual review: natural catastrophes 2002*. Munchener Ruck Munich Reinsurance Company, 2002.
- [2] *Megacities-megarisks*. Munich Reinsurance Company, 2004.
- [3] H. Miyatake and A. Nunomura. General overviews and future perspectives of disaster information systems in Japan. *Proceedings of the 35th Joint Meeting of U.S.–Japan Panel on Wind and Seismic Effects*, UJNR, 2003.
- [4] D. Kubo, T. Kobayashi, J. Bayod, Y. Hatsutori, T. Maki, Y. Hasegawa, and S. Suzuki. Low-cost aerial photography system using ducted fan VTOL aerial robots. *Proceedings of the 44th aircraft symposium*, Omiya, Japan, 1E8, pp. 309–314, 2006. (in Japanese)
- [5] E. N. Johnson and M. A. Turbe. Modeling, control, and flight testing of a small ducted fan aircraft. *AIAA Guidance, Navigation, and Control Conference and Exhibit*, San Francisco, California, 2005.
- [6] *MicroPilot autopilot installation and operation*. MicroPilot Inc., 2005.

**Copyright Statement**

The authors confirm that they, and/or their company or institution, hold copyright on all of the original material included in their paper. They also confirm they have obtained permission, from the copyright holder of any third party material included in their paper, to publish it as part of their paper. The authors grant full permission for the publication and distribution of their paper as part of the ICAS2008 proceedings or as individual off-prints from the proceedings.

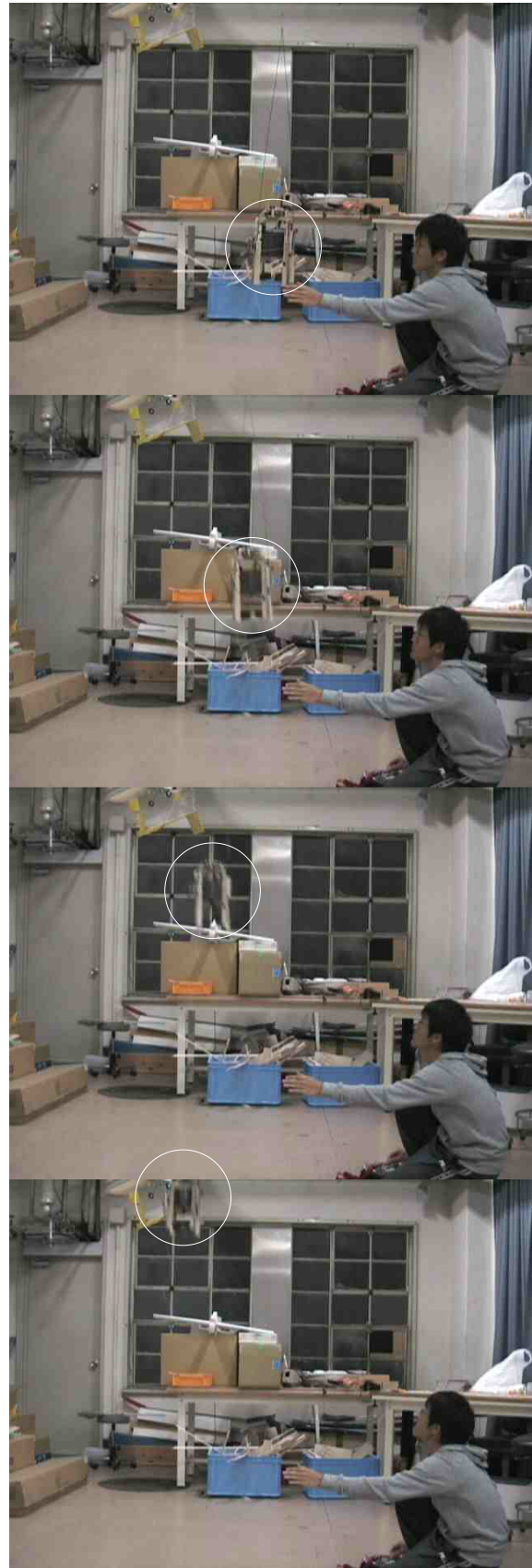


**Fig. 10** A sequence of freeze-frame pictures of the flight testing